scientific reports

Check for updates

OPEN

NIPAL4 is an important marker for clear cell renal cell carcinoma prognosis and immunotherapy

Shuyan Wei[1,6,7], Fang Lyu[2,7], Bei Qian[3,7], Yumei Tang[4]✉ & Qingliu He[5]✉

Clear cell renal cell carcinoma (ccRCC) poses significant clinical challenges due to its high metastatic rate at diagnosis and resistance to conventional therapies. The magnesium transporter NIPAL4, involved in lipid metabolism and magnesium ion homeostasis, has recently been implicated in cancer biology but remains understudied in ccRCC. In this study, we identifies NIPAL4 as a potential prognostic marker and therapeutic target in ccRCC. High NIPAL4 expression is associated with poor prognosis and contributes to tumor proliferation and migration. Bioinformatics analyses indicate that NIPAL4 is involved in critical pathways related to the extracellular matrix, lipid metabolism, and the TGF-β signaling pathway. Moreover, NIPAL4's association with immune cell infiltration and immune checkpoint molecules highlights its potential as an immunotherapy marker. These findings warrant further investigation into NIPAL4's role in ccRCC to develop more effective treatment strategies.

Renal cell carcinoma (RCC) represents a significant global health challenge, accounting for more than 330,000 new cancer cases and over 140,000 cancer-related deaths annually[1,2]. Clear cell renal cell carcinoma (ccRCC) is the most prevalent subtype, constituting approximately 75-80% of all RCC cases[3,4]. The clinical management of ccRCC is particularly problematic due to its high incidence of metastasis at initial diagnosis, occurring in about 30% of patients, and its notable resistance to conventional chemotherapies and radiotherapies[5,6]. This resistance underscores the critical need for innovative prognostic markers and therapeutic targets[7–9].

The magnesium transporter NIPAL4 (NIPA-like domain containing 4) has recently emerged as a significant protein in the broader landscape of biology[10–12]. NIPAL4 is known for its essential role in the metabolism of epidermal lipids and the homeostasis of magnesium ions (Mg^{2+}), which function as secondary messengers in various cellular processes[13–15]. Mg^{2+} is intricately linked to the proliferation, metabolic reprogramming, and apoptosis resistance of tumor cells[16,17]. While mutations in NIPAL4 have been associated with autosomal recessive congenital ichthyosis, a rare dermatological condition characterized by hyperkeratosis, the role of NIPAL4 in oncogenesis, particularly in kidney cancer, remains underexplored[18].

Recent studies have begun to elucidate the involvement of NIPAL4 in the tumor microenvironment, particularly in BRAF-mutated papillary thyroid carcinoma (PTC)[19]. These findings suggest that NIPAL4 might play a broader role in cancer biology, potentially influencing tumor progression and immune interactions. However, there is a lack of comprehensive research on the prognostic value and specific role of NIPAL4 in ccRCC[20–22].

Given this background, our study aims to thoroughly investigate the prognostic, functional, and immunological significance of NIPAL4 in ccRCC. By leveraging extensive datasets from The Cancer Genome Atlas (TCGA) and other sources, we seek to elucidate the expression patterns of NIPAL4 across various cancers, with a focus on its upregulation in ccRCC. We also aim to explore the correlations between NIPAL4 expression and clinical outcomes, including overall survival (OS), TNM staging, and histological grading. Additionally, we will perform functional assays to validate the role of NIPAL4 in tumor proliferation and migration, as well as bioinformatics analyses to uncover the molecular pathways associated with its expression.

[1]Department of Traditional Chinese Medicine and Acupuncture, Renmin Hospital, Hubei University of Medicine, Shiyan, Hubei 442000, P.R. China. [2]Department of Urolgoy, Union Hospital, Tongji Medical College, Tongji Medical College, Huazhong University of Science and Technology, No.1277 jiefang Avenue, Wuhan 430022, China. [3]Department of Thyroid and Breast Surgery, Tongji Medic al College, Union Hospital, Huazhong University of Science and Technology, 1277 jiefang Avenue, Wuhan 430022, China. [4]Department of Nephrology, Meishan Second People's Hospital, Renshou, Meishan, China. [5]Department of Urology, The Second Affiliated Hospital of Fujian Medical University, Quanzhou, China. [6]Chengdu University of Traditional Chinese Medicine, ChengDu, China. [7]Shuyan Wei, Fang Lyu and Bei Qian contributed equally to this work. ✉email: 526673604@qq.com; Heqingliu@fjmu.edu.cn

This comprehensive approach is designed to provide new insights into the potential of NIPAL4 as a prognostic marker and therapeutic target in ccRCC, thereby contributing to the development of more effective treatment strategies for this challenging disease.

Methods

Bioinformatic data collection and processing

In this study, RNA-sequencing data from patients with ccRCC were sourced from TCGA in raw count format. These data were then processed using R software to convert them into Transcripts Per Kilobase Million (TPM), ensuring an accurate representation for subsequent analyses. Concurrently, pertinent clinical information including cancer stage, patient age, and survival duration was also extracted from TCGA to facilitate a comprehensive analysis. Rigorous bioinformatic methodologies were applied to enhance the reliability of the analysis, including the elimination of duplicate patient samples.

This study conducted a detailed examination of NIPAL4 expression in ccRCC samples compared to normal controls using the processed data from the TCGA-KIRC cohort. Visualization of the data was achieved with the ggplot2 package in R, and statistical analyses were performed using the stats package. Furthermore, the expression patterns of NIPAL4 across a variety of cancer types—including bladder cancer, breast cancer, cervical squamous cell carcinoma, cholangiocarcinoma, and colon adenocarcinoma—were explored. This research also delved into the variation of NIPAL4 expression across different cancer stages, leveraging clinical data.

To assess the diagnostic efficacy of NIPAL4 in ccRCC, receiver operating characteristic (ROC) curve analysis was employed, facilitated by the pROC package in R. This comprehensive approach allowed for a nuanced understanding of NIPAL4's role across multiple cancer contexts.

Prognostic significance of NIPAL4 and gene set enrichment analysise

In the TCGA-KIRC cohort, patients were classified into NIPAL4-High and NIPAL4-Low groups based on their NIPAL4 expression status. Kaplan-Meier analysis, utilizing the 'survival' and 'surminer' R packages, was performed to evaluate prognostic indicators among these groups. To account for the influence of other clinically relevant parameters, both univariate and multivariate Cox regression analyses were conducted using the 'survival' and 'rms' R packages. Furthermore, Gene Ontology (GO), Kyoto Encyclopedia of Genes and Genomes (KEGG), and Gene Set Enrichment Analysis (GSEA) was employed to explore potential functional implications of NIPAL4 expression, utilizing the 'clusterprofiler' R package.

The construction of Nomogram、Time-dependent ROC and calibration curve

The prognostic nomogram, time dependent ROC and calibration curve were constructed using the survival (version 3.3-1), timeROC and rms (version 6.3-0) packages. The nomogram integrated clinical variables such as pathological T stage, pathological N stage, and expression status of to predict OS for patients with ccRCC. The time. The time dependent ROC assess the ability of NIPAL4 to predict patient prognosis over different time intervals. The calibration curve is used to assess the discrepancy between the model's predictive performance and the actual observed outcomes.

The association between NIPAL4 and tumor mutation burdern (TMB) and microsatellite instability (MSI)

We also downloaded the Level 4 Simple Nucleotide Variation dataset processed with MuTect2 software (DOI: https://doi.org/10.1038/nature08822) from the GDC portal (https://portal.gdc.cancer.gov/). Utilizing the 'tmb' function in the R package 'maftools' (version 2.8.05), we calculated the TMB for each tumor. We integrated the TMB data with gene expression profiles and applied a $\log_2(x+0.001)$ transformation to each expression value. Additionally, we excluded cancer types with fewer than three samples, ultimately obtaining expression data for 37 different cancer types. Finally, we calculated the Pearson correlation between NIPAL4 and TMB as well as MSI within each type of tumor.

Exploring the relationship between NIPAL4 expression and the level of immune cell infiltration in tumor tissues

Using the TIMER method from the R package IOBR (version 0.99.9, NCBI; DOI:https://doi.org/10.1158/0008-5472. CAN-17-0307), which is dedicated to the comprehensive analysis of tumor-infiltrating immune cells, we re-evaluated the infiltration scores of B cells, CD4 T cells, CD8 T cells, neutrophils, macrophages, and dendritic cells (DCs) for each patient across their respective tumors based on gene expression data. This analysis yielded immune cell infiltration scores for 9,406 tumor samples across 38 distinct tumor types. Subsequently, using the corr.test function from the R package psych (version 2.1.6), we calculated Pearson's correlation coefficients to identify significant correlations between gene expressions and immune cell infiltration scores across the various tumor types.

Cell culture and animals

The human clear cell renal cell carcinoma cells 786O and HK2 cells were obtained from Immocell Biotechnology Co., Ltd. (Xiamen China). 786O cells were cultured in RPMI 1640 with fetal bovine serum (10%), streptomycin (100 μg mL^{-1}) and penicillin (100 U mL^{-1}) at 37℃ in the incubator in 5% CO2 and 21% O2, respectively. HK2 cells were cultured in Dulbecco's Modified Eagle Medium (DMEM) with fetal bovine serum (10%), streptomycin (100 μg mL^{-1}) and penicillin (100 U mL^{-1}) at 37℃ in the incubator in 5% CO2 and 21% O2, respectively.

Nude mice (20 ± 1 g) were provided by Shulaibao (Wuhan) Biotechnology Co., Ltd. (China). All animals were placed in animal facilities with specific pathogen-free conditions at the Laboratory Animal Center of Tongji Medical College, Huazhong University of Science and Technology.

Western blot analysis

786O and HK2 cells were cultured in 6-well plates at a density of 10^6 cells per well for 24 h. The cells were then harvested and lysed on ice using RIPA buffer for 30 min. The lysates were centrifuged at 14,000 g for 10 min at 4 °C, and the supernatant was collected for subsequent analysis. The protein concentration was determined using a BCA assay. Subsequently, the supernatant was subjected to SDS–polyacrylamide gel electrophoresis. The separated proteins were transferred onto a polyvinylidene difluoride membrane at 400 mA for 30 min at 4 °C. The membrane was then washed twice with Tris-buffered saline containing Tween 20 (TBS-T) and blocked with 5% milk for 1 h at room temperature. Following blocking, the membrane was incubated overnight at 4 °C with the NIPAL4 primary antibody, followed by three washes with TBS-T. The membrane was then incubated with goat anti-rabbit IgG (H + L) secondary antibody for 1 h. The immunoreactive bands were detected using Radiance Q chemiluminescent ECL substrate (Azure Biosystems) and visualized with an Amersham ImageQuant 800 biomolecular imager.

Downregulation NIPAL4 in 786O cells

Subsequently, three distinct siRNAs were employed to knockdown NIPAL4 expression in the 786O cells according to the manufacturer's protocol. Following siRNA transfection, the medium was replaced after 24 h, and the cells were further incubated in complete medium for an additional 48 h.

Proliferation assay of 786O cells

Following a 24-hour knockdown of NIPAL4 expression in 786O cells using siRNA-2, the treated cells were seeded into 96-well plates at a density of 2 × 10^3 cells per well. Cell viability was assessed every 24 h using the Cell Counting Kit-8 (CCK-8) assay. The absorbance at OD450 was measured with a microplate reader to determine cell viability in each well.

Wound healing assay of 786O cells

786O cells were seeded in 6-well plates and cultured until they reached near confluence. After a 24-hour knockdown of NIPAL4 expression using siRNA-2, a straight scratch was made in each well using a 200 µL pipette tip, and images were captured. The cells were then cultured in serum-free medium for 24 h to induce starvation. The wound closure was observed and documented by capturing images at the specified time points.

In vivo proliferation assay of NIPAL4 knockdown in nude mice

Stable 786O cells with NIPAL4 knockdown were established using shRNA. The cells were digested and collected for injection. 786O tumor cells (1 × 10^7 cells per mouse) were injected into the right axilla of nude mice ($n = 5$). Tumor volume was measured daily starting from the 5th day post-inoculation until the 15th day. On the 15th day, the mice were sacrificed through cervical dislocation, and the tumor tissues were excised and photographed. Guidelines for Ethical Review of Laboratory Animal Welfare in China (GB/T 35892-2018) require that effective anesthesia should be provided during surgery and dissection of live animals, including those with motor paralysis. In our experiments, nude mice were injected subcutaneously only, no anesthesia was required. All experimental protocols have been approved by the Medical Ethics Committee, The Second Affiliated Hospital of Fujian Medical University, Fuzhou, China (No. 2021-51). We confirm that all experiments were performed in accordance with relevant named guidelines and regulations (GB/T 35892-2018) and comply with the ARRIVE guidelines.

SiRNA and ShRNA sequences

The siRNA used in this study include siRNA-1: sense 5′-GCACAGUGAUGGUGAUACATT; antisense 5′-UGUAUCACCAUCACUGUGCTT, siRNA-2: sense 5′-GAAGAGAAACCCAAAGUAUTT; antisense 5′-AUACUUUGGGUUUCUCUUCTT, siRNA-3: sense 5′-CAACAGAGCACUGGACAUUTT; antisense 5′-AAUGUCCAGUGCUCUGUUGTT. The shRNA used in this study sequences was sense 5′-GAAGAGAAACCCAAAGUAUTT; antisense 5′-AUACUUUGGGUUUCUCUUCTT.

Results

NIPAL4 mRNA expression levels and their relationship with overall survival in clear cell renal cell carcinoma

NIPAL4 is highly expressed in various tumors, and in ccRCC, its mRNA expression levels in both paired and unpaired samples from KIRC (Kidney Renal Clear Cell Carcinoma) are significantly higher than in normal tissues (Fig. 1A,B). By constructing ROC curves, this study finds that the expression level of NIPAL4 can effectively differentiate ccRCC tissues from normal tissues (Fig. 1C). Based on the median expression level of NIPAL4, patients were categorized into high and low expression groups for survival analysis. Kaplan-Meier curves indicate that in the TCGA database, the OS of the high NIPAL4 expression group is significantly poorer than that of the low expression group (Fig. 1D). These results suggest that NIPAL4 acts as an oncogene and is significantly associated with the prognosis of patients with clear cell renal cell carcinoma.

Clinical pathological variables and overall survival correlate with NIPAL4 expression

Using independent sample t-tests to evaluate the clinical significance of NIPAL4 expression levels, we found significant correlations between NIPAL4 expression and various clinical parameters such as TNM staging, gender, clinical pathological staging, and histological grading (Fig. 2A–F). Univariate Cox regression analysis revealed that NIPAL4 expression is positively associated with TNM stage, pathological grade, and age in patients with ccRCC (Fig. 2G). Additionally, multivariate Cox regression analysis indicate that higher NIPAL4 expression, pathologic M stage and age were associated with poorer overall survival of ccRCC patients (Fig. 2H). These

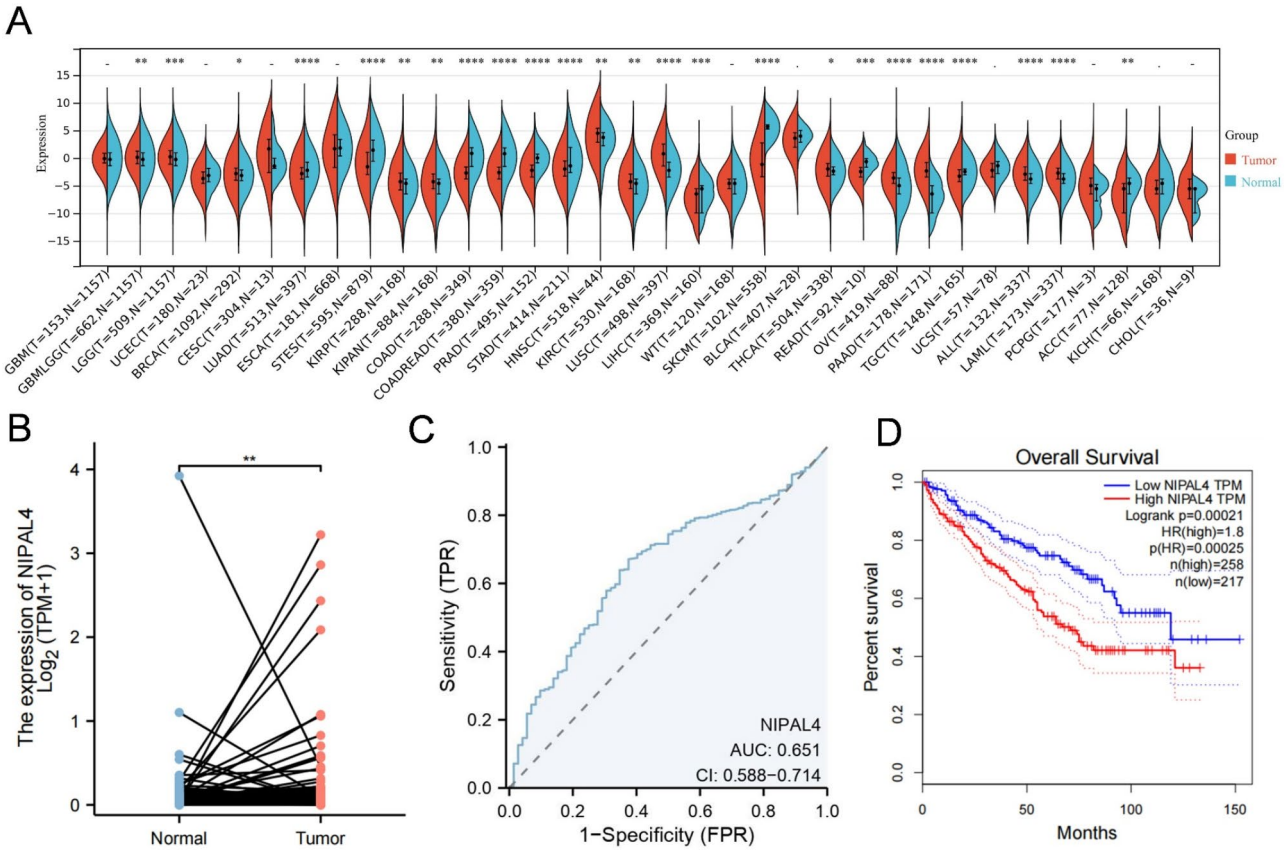

Fig. 1. NIPAL4 mRNA expression levels and their relationship with overall survival in ccRCC. (**A**) Violin plots showing the expression levels of NIPAL4 across various tumor types. The expression levels in tumor tissues (red) and normal tissues (blue) are compared, indicating a significant overexpression of NIPAL4 in many tumor types, including ccRCC. Statistical significance is indicated by asterisks (*$p < 0.05$, **$p < 0.01$, ***$p < 0.001$, ****$p < 0.0001$). (**B**) Paired analysis of NIPAL4 expression in normal (blue) and tumor (red) tissues from ccRCC patients. The expression of NIPAL4 is significantly higher in tumor tissues compared to matched normal tissues ($p < 0.01$). (**C**) Receiver Operating Characteristic (ROC) curve analysis of NIPAL4 expression for differentiating ccRCC tissues from normal tissues. The Area Under the Curve (AUC) value is 0.651, indicating moderate diagnostic performance. (**D**) Kaplan-Meier survival curves for OS based on NIPAL4 expression levels in ccRCC patients from the TCGA database. Patients were divided into high (red) and low (blue) NIPAL4 expression groups based on the median expression level. High NIPAL4 expression is significantly associated with poorer overall survival (log-rank $p = 0.0021$).

findings indicate a substantial correlation between NIPAL4 expression and the clinical pathology of ccRCC, suggesting that NIPAL4 may serve as a significant prognostic biomarker for this disease.

Functional validation of NIPAL4

The 786O renal ccRCC was selected for functional validation experiments of NIPAL4. Initially, We test NIPAL4 expression between normal renal cell line (HK2) and renal tumor cell line (786O). NIPAL4 express higher in 786O than HK2 (Fig. 3A,B). NIPAL4 expression in the 786O cell line was silenced using siRNA, with successful downregulation confirmed by Western blot analysis (Fig. 3C,D). The impact of NIPAL4 on cell migration was also demonstrated using a scratch assay in cells treated with siNIPAL4-2, highlighting its close association with the migration of renal clear cell carcinoma cells (Fig. 3E). The silencing of NIPAL4 in 786O cells significantly inhibited cell proliferation, indicating that NIPAL4 plays a role in regulating the proliferation rate of renal clear cell carcinoma (Fig. 3F). Furthermore, the proliferation rate of renal clear cell carcinoma cells with silenced NIPAL4 was notably suppressed in vivo in nude mice (Fig. 3G,H). These findings collectively suggest that NIPAL4 is a key regulator of both the proliferation and migration of renal clear cell carcinoma cells, supporting its potential as a therapeutic target.

Development of a prognostic nomogram for clear cell renal cell carcinoma

By constructing a nomogram that incorporates clinical-pathological variables along with NIPAL4 expression, we introduced a quantitative method for predicting prognostic risk (Fig. 4A). ROC analysis was conducted to ascertain the prognostic value of NIPAL4 expression in clear cell renal cell carcinoma, where the AUC values for NIPAL4 expression were 0.673, 0.643, and 0.652(Figure 4B). Additionally, we verified the consistency between

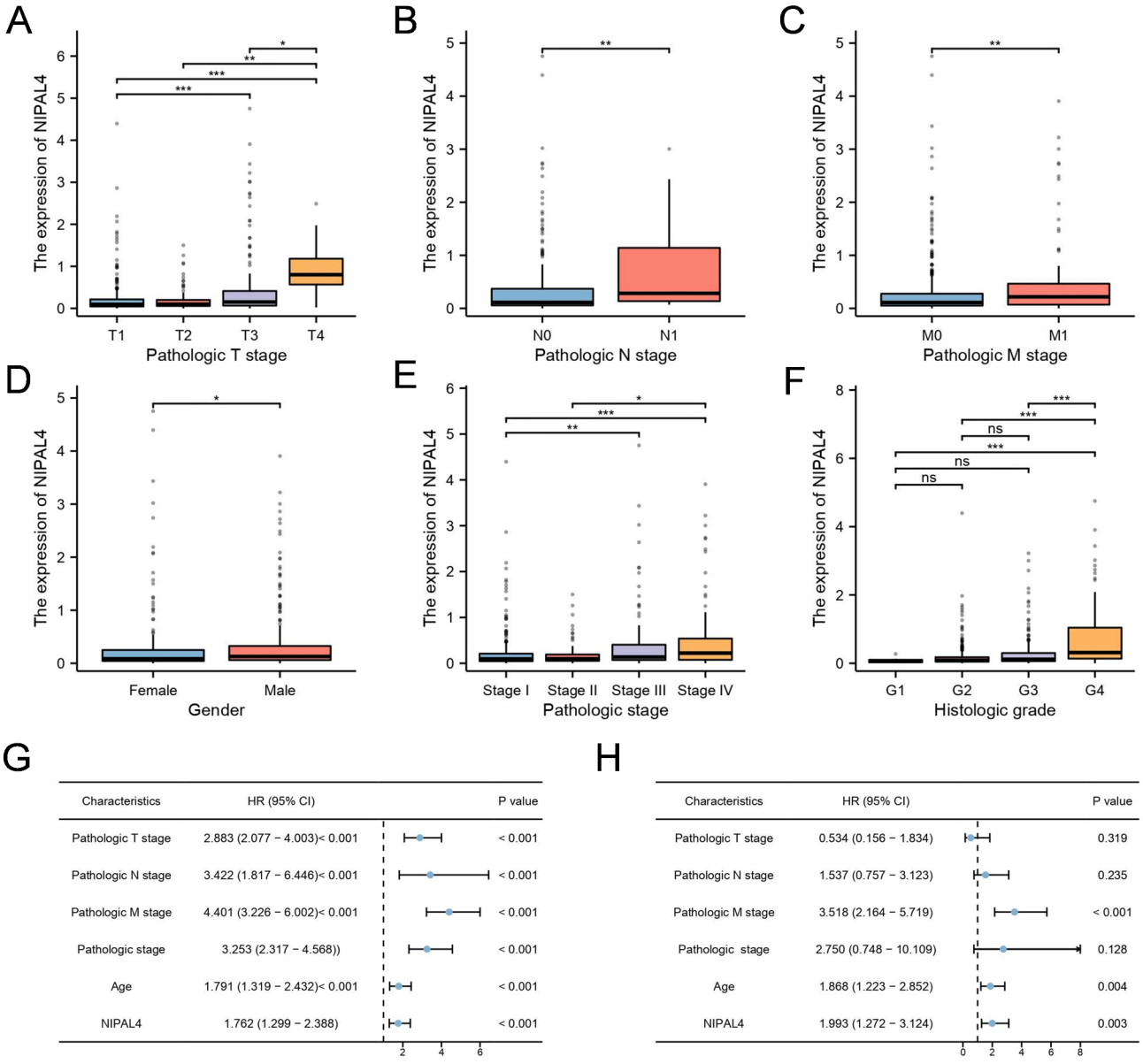

G

Characteristics	HR (95% CI)	P value
Pathologic T stage	2.883 (2.077 − 4.003)	< 0.001
Pathologic N stage	3.422 (1.817 − 6.446)	< 0.001
Pathologic M stage	4.401 (3.226 − 6.002)	< 0.001
Pathologic stage	3.253 (2.317 − 4.568))	< 0.001
Age	1.791 (1.319 − 2.432)	< 0.001
NIPAL4	1.762 (1.299 − 2.388)	< 0.001

H

Characteristics	HR (95% CI)	P value
Pathologic T stage	0.534 (0.156 − 1.834)	0.319
Pathologic N stage	1.537 (0.757 − 3.123)	0.235
Pathologic M stage	3.518 (2.164 − 5.719)	< 0.001
Pathologic stage	2.750 (0.748 − 10.109)	0.128
Age	1.868 (1.223 − 2.852)	0.004
NIPAL4	1.993 (1.272 − 3.124)	0.003

Fig. 2. Clinical Pathological Variables and Overall Survival Correlate with NIPAL4 Expression. (**A**) Box plot illustrating the expression of NIPAL4 across different pathological T stages (T1, T2, T3, T4) in ccRCC. NIPAL4 expression is significantly higher in more advanced T stages (*$p < 0.05$, **$p < 0.01$, ***$p < 0.001$). (**B**) Box plot showing NIPAL4 expression across pathological N stages (N0, N1) in ccRCC. Higher NIPAL4 expression is observed in N1 stage compared to N0 stage (**$p < 0.01$). (**C**) Box plot depicting NIPAL4 expression across pathological M stages (M0, M1) in ccRCC. NIPAL4 expression is significantly elevated in M1 stage compared to M0 stage (**$p < 0.01$). (**D**) Box plot comparing NIPAL4 expression between female and male ccRCC patients. No significant difference is observed. (**E**) Box plot demonstrating NIPAL4 expression across different pathological stages (Stage I, Stage II, Stage III, Stage IV) in ccRCC. Higher NIPAL4 expression is seen in more advanced stages (**$p < 0.01$, ***$p < 0.001$). (**F**) Box plot showing NIPAL4 expression across different histological grades (G1, G2, G3, G4) in ccRCC. Higher NIPAL4 expression is observed in higher histological grades (**$p < 0.01$, ***$p < 0.001$, ns = not significant). (**G**) Forest plot from univariate Cox regression analysis showing the hazard ratios (HR) and 95% confidence intervals (CI) for the association between NIPAL4 expression and clinical pathological variables (TNM stage, pathological grade, age) with overall survival in ccRCC patients. (**H**) Forest plot from multivariate Cox regression analysis showing the hazard ratios (HR) and 95% confidence intervals (CI) for the association between NIPAL4 expression and clinical pathological variables (TNM stage, pathological grade, age) with overall survival in ccRCC patients.

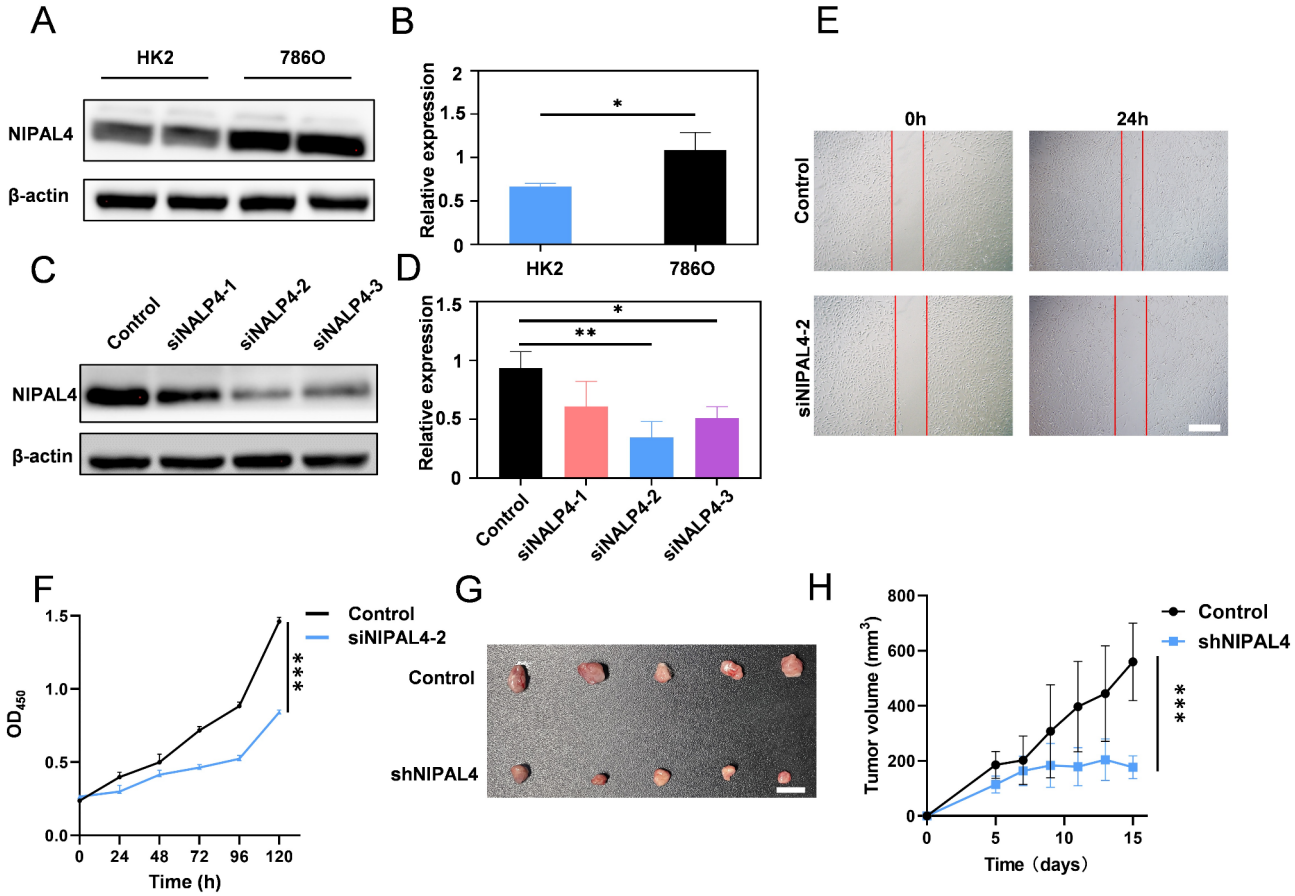

Fig. 3. Functional validation of NIPAL4. (**A**) Western blot analysis showing the NIPAL4 expression between normal kidney cell line (HK2) and ccRCC (786O). (**B**) The statistics of NIPAL4 expression. Student's t-test was performed to determine the statistical significance of the data ($*p < 0.05$, $n = 3$). Data are presented as mean ± SD. (**C**) Western blot analysis showing NIPAL4 expression in 786O renal clear cell carcinoma cells transfected with three different siRNAs (siNIPAL4-1, siNIPAL4-2, siNIPAL4-3). (**D**) The statistics of expression after knockdown NIPAL4 by siRNA. Student's t-test was performed to determine the statistical significance of the data ($*p < 0.05$, $**p < 0.01$, $n = 3$). Data are presented as mean ± SD. (**E**) Wound healing assay images showing the migration of 786O cells treated with siNIPAL4-2 compared to the control at 0 h and 24 h. Knockdown of NIPAL4 reduced the migration ability of 786O cells. Scale bar = 100 µm. (**F**) Cell proliferation assay of 786O cells following NIPAL4 knockdown. Cell viability was measured at different time points (0, 24, 48, 72, 96, 120 h) using the Cell Counting Kit-8 (CCK-8) assay. Student's t-test was performed to determine the statistical significance of the data ($*p < 0.05$, $**p < 0.01$, $***p < 0.001$, $n = 5$). Data are presented as mean ± SD. (**G**) Representative images of tumors excised from nude mice injected with 786O cells transfected with siNIPAL4 and control ($n = 5$). Tumors were harvested 15 days post-injection. Scale bar = 1 cm. (**H**) Tumor growth curve showing the volume of tumors in nude mice injected with shNIPAL4-transfected 786O cells compared to control over a period of 15 days. Knockdown of NIPAL4 significantly suppressed tumor growth in vivo. Student's t-test was performed to determine the statistical significance of the data ($*p < 0.05$, $**p < 0.01$, $***p < 0.001$, $n = 5$). Data are presented as mean ± SD.

actual and ideal values for 1-year, 3-year and 5-year prognosis (Fig. 4C–E). These findings suggest that combining NIPAL4 with other parameters serves as a predictive marker for estimating OS in patients with clear cell renal cell carcinoma, indicating that our nomogram can predict survival rates with moderate accuracy.

Identification of NIPAL4-Associated signaling pathways

Based on the median expression level of NIPAL4, samples were divided into high and low expression groups, and subjected to GO and KEGG enrichment analyses to identify pathways potentially associated with NIPAL4. The GO enrichment results indicated significant associations of NIPAL4 with processes such as extracellular matrix organization, keratinization, and structures including the collagen-containing extracellular matrix and ion channel complexes (Fig. 5A). The KEGG analysis revealed that NIPAL4 is significantly linked to pathways like protein digestion and absorption, ECM-receptor interaction, cytokine-cytokine receptor interaction, TGF-beta signaling pathway, and metabolism of xenobiotics by cytochrome P450 (Fig. 5B). Furthermore, Gene Set Enrichment Analysis (GSEA) highlighted the most enriched pathways based on normalized enrichment scores (NES) and nominal p-values less than 0.05, showing NIPAL4's involvement in various extracellular matrix

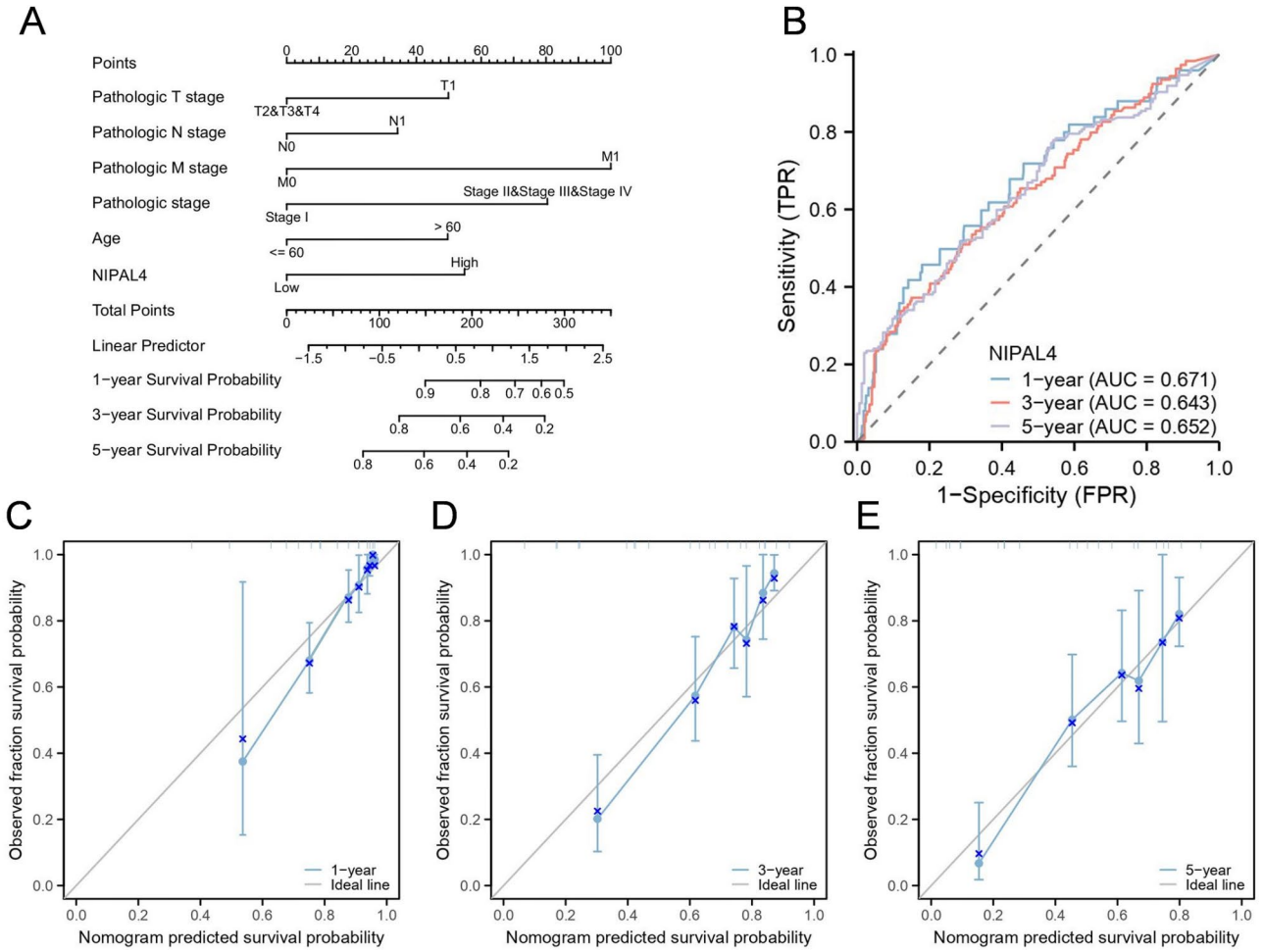

Fig. 4. Development of a prognostic nomogram for clear cell renal cell carcinoma. (**A**) Nomogram incorporating clinical-pathological variables along with NIPAL4 expression to predict OS in patients with ccRCC. Variables included in the nomogram are pathological T stage, pathological N stage, pathological M stage, pathological stage, age and NIPAL4 expression. (**B**) Receiver Operating Characteristic (ROC) curves for 1-year, 3-year, and 5-year survival probabilities based on the nomogram. The AUC values for NIPAL4 expression are 0.671 for 1-year, 0.643 for 3-year, and 0.652 for 5-year survival, indicating moderate predictive accuracy. (**C**) Calibration curve for 1-year survival probability, showing the consistency between predicted and observed survival rates. The blue dots represent the actual survival rates, and the dashed line represents the ideal prediction. (**D**) Calibration curve for 3-year survival probability, illustrating the agreement between the nomogram-predicted survival probability and the observed survival rates. (**E**) Calibration curve for 5-year survival probability, demonstrating the consistency between predicted and observed survival probabilities, confirming the accuracy of the nomogram over different time intervals.

signaling pathways such as ECM regulators, extracellular matrix organization, and collagen formation, along with pathways like proinflammatory and profibrotic mediators, valine, leucine, and isoleucine degradation, and peroxisomal lipid metabolism (Fig. 5C–J).

Association of NIPAL4 with PPI, TMB, and MSI

The protein-protein interaction (PPI) network indicates that NIPAL4 is significantly associated with ten different genes: PI4K2B, SLC27A4, CERS3, ALOXE3, CYP4F22, TGM1, PNPLA1, ALOX12B, LIPN, and ADCA12 (Fig. 6A). Furthermore, we examined the relationship between NIPAL4 and both TMB and MSI across various tumors. The results demonstrated that NIPAL4 is negatively correlated with TMB and MSI levels in multiple types of tumors (Fig. 6B-C). However, in ccRCC, NIPAL4 showed no significant association with TMB and MSI levels.

Association of NIPAL4 with immune infiltration, tumor microenvironment, and immune checkpoint molecules

Based on enrichment analysis, we investigated the relationship between NIPAL4 and immune cell infiltration. In ccRCC, the TIMER2.0 database revealed a strong negative correlation between NIPAL4 and tumor purity. This suggests that higher NIPAL4 expression is associated with greater infiltration of various cells within the tumor.

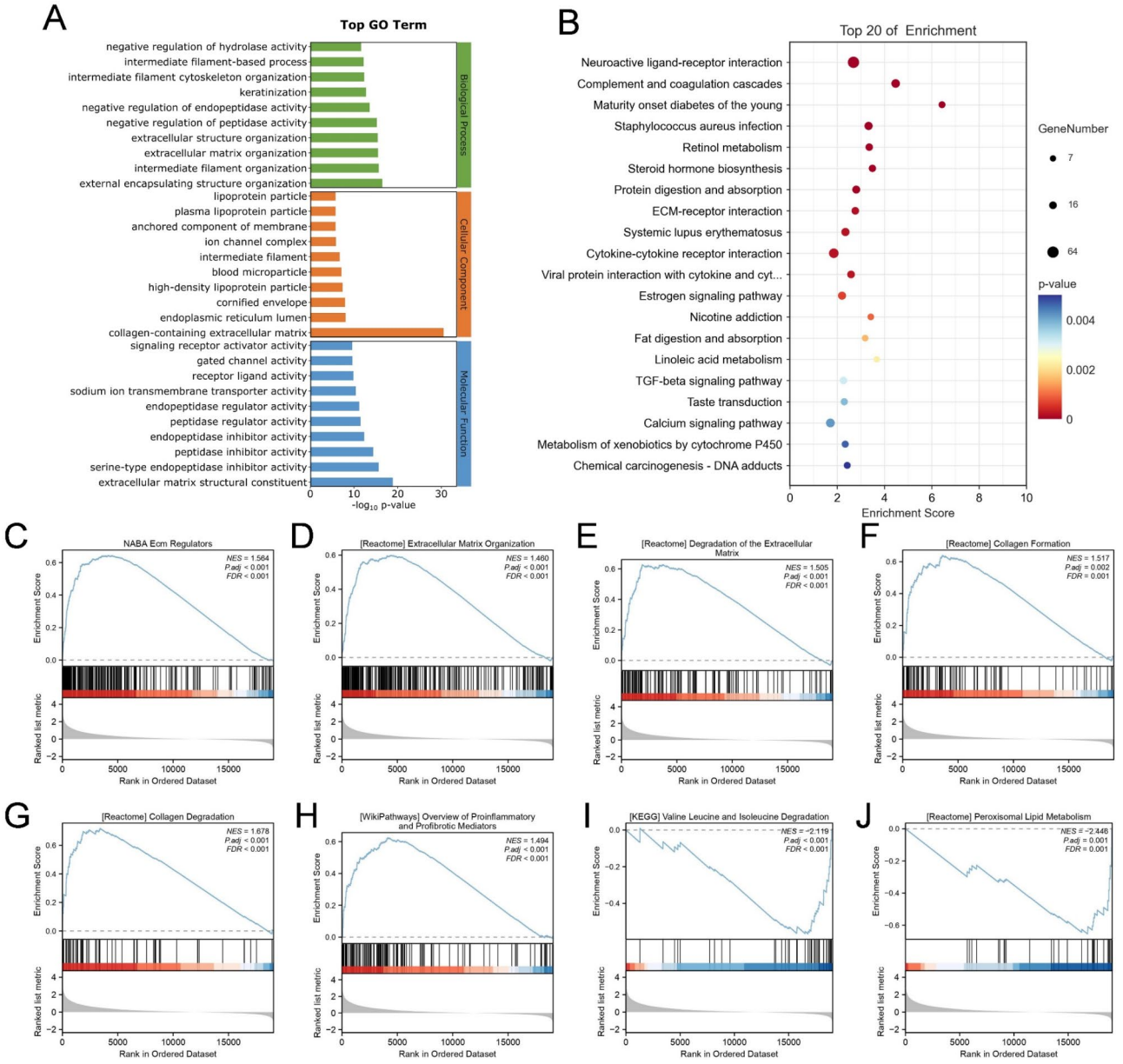

Fig. 5. Identification of NIPAL4-associated signaling pathways. (**A**) GO enrichment analysis of differentially expressed genes based on NIPAL4 expression levels. The top GO terms are related to extracellular matrix organization, keratinization, and ion channel complexes. (**B**) KEGG pathway analysis of genes associated with NIPAL4. Top enriched pathways include protein digestion and absorption, ECM-receptor interaction, cytokine-cytokine receptor interaction, and the TGF-beta signaling pathway. (**C**–**J**) Gene Set Enrichment Analysis (GSEA) highlighting the most enriched pathways based on normalized enrichment scores (NES) and nominal p-values less than 0.05.

Further analysis revealed that NIPAL4 expression is positive correlated with the infiltration of CD4 + T cells, macrophages, neutrophils and dendritic cells (DCs) (Fig. 7A). Using TCGA database, we analyzed the impact of NIPAL4 on immune infiltration in ccRCC. The results indicated that the infiltration levels of CD8 + T cells, neutrophils, macrophages, and DCs are positively correlated with NIPAL4 expression (Fig. 7B). Moreover, our study identified significant correlations between NIPAL4 and various immune checkpoint molecules in ccRCC, including IL10, CD274 (PD-L1), CTLA4, TIGIT, and ADORA2A (Fig. 7C). Based on the aforementioned data, it can be inferred that patients displaying high levels of NIPAL4 expression could potentially have a more favorable response to immune checkpoint inhibitor therapy.

Discussion

In this study, we first established that NIPAL4 is highly expressed across various tumors. Specifically, in ccRCC, NIPAL4 expression is higher in tumor tissues compared to paired adjacent normal tissues, and patients with

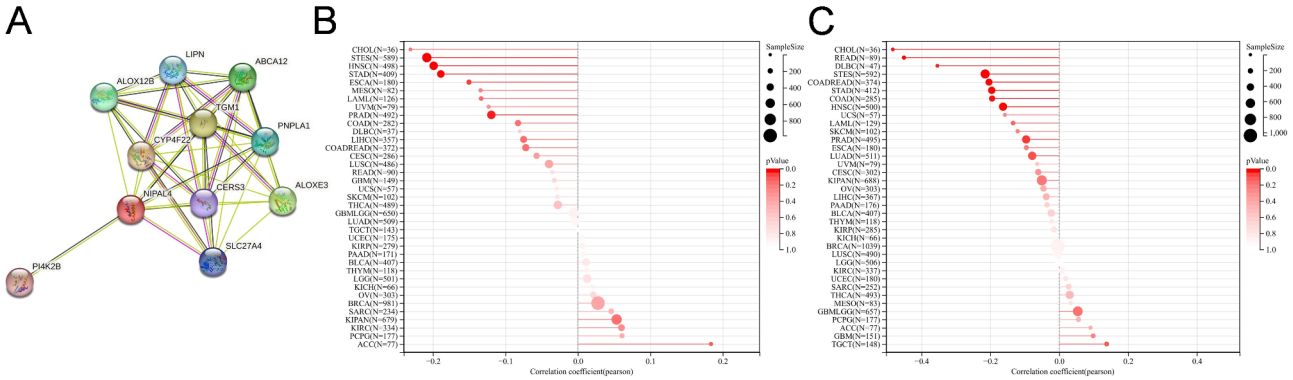

Fig. 6. Association of NIPAL4 with PPI, TMB, and MSI. (**A**) Protein-protein interaction (PPI) network illustrating the significant associations of NIPAL4 with ten different genes: PI4K2B, SLC27A4, CERS3, ALOXE3, CYP4F22, TGM1, PNPLA1, ALOX12B, LIPN, and ADCA12. (**B**) Correlation analysis between NIPAL4 expression and TMB across various tumor types. The plot demonstrates a negative correlation between NIPAL4 and TMB levels in multiple types of tumors. (**C**) Correlation analysis between NIPAL4 expression and MSI across various tumor types. The plot indicates a negative correlation between NIPAL4 and MSI levels in multiple types of tumors. However, in ccRCC, NIPAL4 showed no significant association with TMB and MSI levels.

high NIPAL4 expression tend to have poorer OS. This differential expression is corroborated by data from the GEO dataset and protein blotting analyses. Furthermore, high NIPAL4 expression in the TCGA database is strongly associated with worse TNM stage, pathological stage, and histological grade in ccRCC. Univariate COX regression analysis revealed a positive correlation between NIPAL4 expression, TNM stage, and patient age. A nomogram integrating NIPAL4 expression with clinicopathological variables showed good predictive performance for 1-year, 3-year, and 5-year mortality, with AUCs of 0.671, 0.643, and 0.652, respectively.

We also performed GO, KEGG, and GSEA analyses on tissues with different levels of NIPAL4 expression to explore its mechanistic role in ccRCC. Our findings indicate that NIPAL4 is closely related to extracellular matrix formation and degradation, collagen formation and degradation, lipid metabolism, and the TGF-β signaling pathway. This suggests that NIPAL4 may influence tumor cell metastasis and the tumor immune microenvironment by affecting the extracellular matrix, which may partly explain the poorer N and M stages in patients with high NIPAL4 expression. The TGF-β signaling pathway is well-documented for its association with tumor development and immune infiltration. In late-stage tumors, the TGF-β pathway promotes cancer progression. Furthermore, the influence of NIPAL4 on the extra-tumoral stroma is evidenced by its promotion of the infiltration of a diverse array of immune cells and its association with multiple immune checkpoints, although NIPAL4 does not impact tumor TMB and MSI levels.

In summary, these findings suggest that NIPAL4 is not only a valuable prognostic marker but also a potential therapeutic target in ccRCC. By targeting NIPAL4, it may be possible to develop novel treatment strategies to improve outcomes for patients with this challenging disease. Future research should focus on further elucidating the molecular mechanisms by which NIPAL4 influences tumor biology and exploring its potential in clinical applications.

However, it is important to acknowledge that our article has a few limitations. First, we solely relied on public tumor databases to study NIPAL4 and did not investigate the underlying mechanisms by which NIPAL4 influences the tumor microenvironment. Additionally, future studies could explore the impact of NIPAL4 on immune checkpoint inhibitor response. Moreover, we suggest conducting a radiogenomic analysis of NIPAL4 to examine the radiological phenotype characteristics in ccRCC[23].

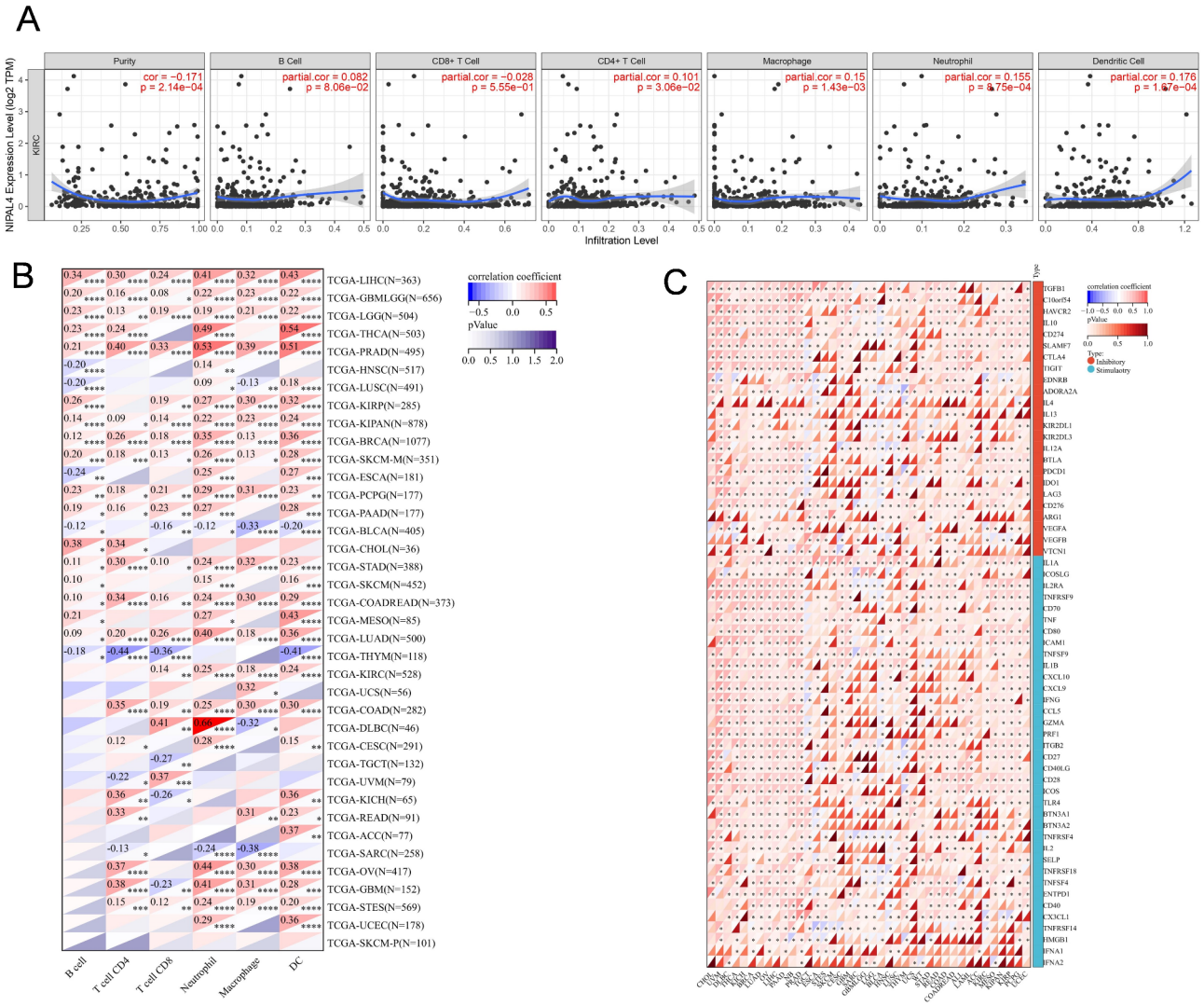

Fig. 7. Association of NIPAL4 with immune infiltration, tumor microenvironment, and immune checkpoint molecules. (**A**) Scatter plots showing the correlation between NIPAL4 expression and various immune cell infiltrations, including B cells, CD8 + T cells, CD4 + T cells, macrophages, neutrophils, and dendritic cells (DCs) in ccRCC. The analysis indicates a strong negative correlation between NIPAL4 expression and immune cell infiltration levels. (**B**) Heatmap displaying the correlation coefficients between NIPAL4 expression and the infiltration levels of different immune cell types across multiple tumor types from the TCGA database. The infiltration levels of CD8 + T cells, neutrophils, macrophages, and DCs are positively correlated with NIPAL4 expression in ccRCC. (**C**) Heatmap illustrating the correlation between NIPAL4 expression and various immune checkpoint molecules in ccRCC, including IL10, CD274 (PD-L1), CTLA4, TIGIT, and ADORA2A. The analysis shows significant correlations, suggesting the potential involvement of NIPAL4 in immune regulation within the tumor microenvironment.

Data availability

The original contributions encompassed in this study are thoroughly documented within the article. For additional information or specific inquiries, readers are encouraged to contact the corresponding author directly.

Received: 5 November 2024; Accepted: 3 March 2025
Published online: 26 March 2025

9.References

1. Znaor, A. et al. International variations and trends in renal cell carcinoma incidence and mortality. *Eur. Urol.* **67**, 519–530 (2015).
2. Hu, M. et al. Global incidence and mortality of renal cell carcinoma in 2020. *Zhonghua Liu Xing Bing Xue Za Zhi = Zhonghua Liuxingbingxue Zazhi*. **44**, 575–580 (2023).
3. Hsieh, J. J. et al. Renal cell carcinoma. *Nat. Reviews Disease Primers.* **3**, 17009 (2017).
4. Kim, I. H. & Lee, H. J. The frontline Immunotherapy-Based treatment of advanced clear cell renal cell carcinoma: Current evidence and clinical perspective. *Biomedicines* 10 (2022).

5. Mollica, V. et al. Resistance to systemic agents in renal cell carcinoma predict and overcome genomic strategies adopted by tumor. *Cancers* 11 (2019).
6. Yang, J., Wang, K. & Yang, Z. Treatment strategies for clear cell renal cell carcinoma: past, present and future. *Front. Oncol.* **13**, 1133832 (2023).
7. Chao, X. et al. Comprehensive analysis of LncRNAs as biomarkers for diagnosis, prognosis, and treatment response in clear cell renal cell carcinoma. *Mol. Therapy Oncolytics*. **22**, 209–218 (2021).
8. Angulo, J. C. et al. The role of epigenetics in the progression of clear cell renal cell carcinoma and the basis for future epigenetic treatments. *Cancers* 13 (2021).
9. Meng, M. et al. Integrative bioinformatics analysis demonstrates the prognostic value of chromatin accessibility biomarkers in clear cell renal cell carcinoma. *Front. Oncol.* **11**, 814396 (2021).
10. Gong, Z. et al. Treatment of autosomal recessive congenital ichthyosis caused by a NIPAL4 variant with Upadacitinib. *J. Eur. Acad. Dermatol. Venereol. JEADV* (2024).
11. Yamaji, M. et al. Alteration of epidermal lipid composition as a result of deficiency in the magnesium transporter Nipal4. *J. Lipid Res.* 100550 (2024).
12. Rossel, S. V. J. et al. Expanding the molecular and clinical spectrum of autosomal recessive congenital ichthyosis caused by pathogenic variants in NIPAL4 and PNPLA1 and evaluation of novel therapeutic interventions. *J. Eur. Acad. Dermatol. Venereol. JEADV*. **37**, e1405–e09 (2023).
13. Li, H. et al. The expression of epidermal lipoxygenases and transglutaminase-1 is perturbed by NIPAL4 mutations: indications of a common metabolic pathway essential for skin barrier homeostasis. *J. Invest. Dermatol.* **132**, 2368–2375 (2012).
14. de Baaij, J. H., Hoenderop, J. G. & Bindels, R. J. Magnesium in man: implications for health and disease. *Physiol. Rev.* **95**, 1–46 (2015).
15. Laadhar, S. et al. Identification of a novel missense mutation in NIPAL4 gene: first 3D model construction predicted its pathogenicity. *Mol. Genet. Genom. Med.* **8**, e1104 (2020).
16. Masui, K., Cavenee, W. K. & Mischel, P. S. mTORC2 in the center of cancer metabolic reprogramming. *Trends Endocrinol. Metab.* **25**, 364–373 (2014).
17. Wolf, F. I. & Trapani, V. Magnesium and its transporters in cancer: A novel paradigm in tumour development. *Clin. Sci.* **123**, 417–47 (2012).
18. Azeez, F. et al. Lamellar ichthyosis with a novel NIPAL4 variant showing dramatic response to high-dose vitamin D therapy. Pediatric dermatology. (2023).
19. Xia, Y. et al. Construction of a tumor immune Microenvironment-Related prognostic model in BRAF-Mutated papillary thyroid Cancer. *Front. Endocrinol.* **13**, 895428 (2022).
20. Rong, Y. et al. Analysis of the potential biological value of pyruvate dehydrogenase E1 subunit B in human cancer. *World J. Gastrointest. Oncol.* **16**, 144–181 (2024).
21. Ke, J., Chen, J. & Liu, X. Analyzing and validating the prognostic value and immune microenvironment of clear cell renal cell carcinoma. *Anim. Cells Syst.* **26**, 52–61 (2022).
22. Dani, K. A. et al. Comprehensive systematic review of biomarkers in metastatic renal cell carcinoma: Predictors, prognostics, and therapeutic monitoring. *Cancers* 15 (2023).
23. Greco, F. et al. Radiogenomic features of GIMAP family genes in clear cell renal cell carcinoma: an observational study on CT images. *Genes* **14**, 1832 (2023).

Author contributions

S.W. was responsible for data curation and writing the initial draft. F.L. handled specimen collection and experiment implementation. B.Q. conducted specific experiments and bioinformatics analysis. Y.T. and Q.H. provided research ideas and served as corresponding author.

Declarations

Competing interests

The authors declare no competing interests.

Additional information

Supplementary Information The online version contains supplementary material available at https://doi.org/10.1038/s41598-025-92811-1.

Correspondence and requests for materials should be addressed to Y.T. or Q.H.